Structural Engineering and Mechanics, *Vol. 70, No. 3 (2019) 279-287*
DOI: https://doi.org/10.12989/sem.2019.70.3.279

Near-tip grid refinement for the effective and reliable natural element crack analysis

J.R. Cho*

Department of Naval Architecture and Ocean Engineering, Hongik University, Jochiwon, Sejong 30016, Korea

(Received September 17, 2018, Revised February 5, 2019, Accepted February 20, 2019)

Abstract. This paper intends to introduce a near-tip grid refinement and to explore its usefulness in the crack analysis by the natural element method (NEM). As a sort of local h-refinement in FEM, a NEM grid is locally refined around the crack tip showing the high stress singularity. This local grid refinement is completed in two steps in which grid points are added and Delaunay triangles sharing the crack tip node are divided. A plane-state plate with symmetric edge cracks is simulated to validate the proposed local grid refinement and to examine its usefulness in the crack analysis. The crack analysis is also simulated using a uniform NEM grid for the sake of comparison. The near-tip stress distributions and SIFs that are obtained using a near-tip refined NEM grid are compared with the exact values and those obtained using uniform NEM grid. The convergence rates of global relative error to the total number of grid points between the refined and non-refined NEM grids are also compared.

Keywords: crack analysis; near-tip grid refinement; natural element method; stress intensity factor; near-tip stress distribution; convergence rate

1. Introduction

The cracked bodies are characterized by the $1/\sqrt{r}$ singularity in their stress and strain fields at the crack tip. This kind of singularity occurs whenever the cornering angle in a non-convex domain is greater than 180°, in order for the deformed elastic body to have finite strain energy (Szabó and Babuška 1991). This geometry-induced stress singularity increases in proportional to the cornering angle, so that the crack tip having 2π cornering angle exhibits the highest singularity. In addition, the singular behavior in the stress field is confined within an extremely small region near the crack tip. For these reasons, the capturing of high gradient in the field towards the crack tip by the numerical method was not a simple task (Tong *et al.* 1973). In fact, the use of limited number of standard finite elements cannot successfully interpolate such a sharp gradient in the displacement field near the crack tip. In this context, the evaluation of stresses near the crack tip has been a continuous challenging subject over several decades.

According to the brief literature survey, the numerical methods for evaluating the stresses at or/and near the crack tip can be classified into direct and indirect approaches. In the former approach, the near-tip stress field is directly approximated using a locally refined FE mesh (Lo and Lee 1992, Solanki *et al.* 2003, Areias *et al.* 2016) or the specially-devised singular elements (Rice and Tracey 1973, Barsoum 1976, Cao and Liu 2012). More recently, Xiao *et al.* (2004) extended the hybrid crack element and Hou *et al.* (2017) improved the extended FEM (XFEM), in order to directly evaluate the stress intensity factors (SIF) and the higher order terms in the asymptotic expansions. Chidgzey and Deeks (2005) applied the scaled boundary FEM to the evaluation of linear elastic crack tip stress fileds. The basic motivation of this approach is to more accurately approximate the near-tip stress field by capturing the high gradient in the near-tip displacement field or by artificially shifting the location of some nodes in standard finite element.

Meanwhile, in the indirect method, the near-tip displacement and stress fields are approximated by calculating SIFs and substituting them into the known asymptotic stress or displacement fields. To calculate the SIFs, the *J*-integral has been widely used by virtue of its high calculation accuracy and the path independence. In case of mixed-mode SIFs, the contour integral is usually recasted into an equivalent domain integral form, called the interaction integral by introducing the weighting function, in order to extract K_I and K_{II}. The path independence is preserved even for non-homogeneous bodies (Erdogan and Wu 1997, Kim and Paulino 2002). The numerical calculation of SIFs were traditionally made by either FEM or boundary element method. But, since the late 1990s, the extension of meshfree method to the calculation of SIFs using the interaction integral has been actively progressed, inspired by the fact that the interpolation functions used for meshfree methods provide high smoothness (Sukumar and Moran 1999).

Belytschko *et al.* (1995) applied the element-free Galerkin (EFG) method to compute the singular stress fields and the SIFs in 2-D fracture problems. Fleming *et al.* (1997)

*Corresponding author, Professor
E-mail: jrcho@hongik.ac.kr

ISSN: 1225-4568 (Print), 1598-6217 (Online)

enriched the EFG method by adding asymptotic fields to the trial basis functions in order to accurately calculate the SIFs with fewer degrees of freedom. Rabczuk and Belytschko (2004) introduced a simplified meshfree method for arbitrary cracks, in which the crack is treated as a collection of cracked particles. Pant *et al.* (2011) introduced a new enrichment criterion for modeling the kinked cracks using the EFG method to compute the SIFs. Ching and Batra (2011) enriched the polynomial basis functions in the meshless local Petrov-Galerkin (MLPG) method with the crack tip singular fields to predict the singular stress fields near a crack tip and the SIFs. Rao and Rahman (2000) applied the EFG method to calculate the SIF and to simulate the crack propagation in 2-D linear fracture problems under mode-I and mixed-mode loading conditions. Shi *et al.* (2013) and Goli *et al.* (2014) enriched the partition-of-unity (POU) method to solve multiple and mixed-mode adiabatic crack problems.

Even though these methods provide the highly smooth interpolation functions, it is widely known that those suffer from the common difficulties in the enforcement of essential boundary condition and the numerical integration. Differing from these grid-point based meshfree methods, the natural element method (NEM) introduced originally by Braun and Sambridge (1995) uses the basis functions defined based on the Voronoi diagram and Delaunay triangulation. The basis functions called by Laplace interpolation functions used in NEM not only exhibit the high smoothness (Sukumar and Moran 1999), but those satisfy the Kronecker delta property. Thanks to the Kronecker delta property and the introduction of Delaunay triangulation, the natural element method does not lead to difficulties in imposing the essential boundary condition and employing the traditional Gauss quadrature rule for the numerical integration (Sukumar *et al.* 1998, Cho and Lee 2006). This method has been refined and extended to solve the important engineering problems in linear and nonlinear solid mechanics including the crack problem by subsequent researchers (Chenesta *et al.* 2011).

As an extension of the previous works on NEM (Cho and Lee 2014, Cho 2016), this paper intends to introduce a near-tip NEM grid refinement and to explore its usefulness in the calculation of SIFs and near-tip stresses. As a sort of local h-refinement in FEM, the near-tip grid refinement is constructed in two steps in which grid points are added and Delaunay triangles sharing the crack tip node are divided. A plane-state plate with symmetric edge cracks is taken for the numerical experiment that explores the usefulness of the proposed grid refinement. The usefulness is examined by comparing the near-tip stress distributions and SIFs with the exact values and those obtained using uniform NEM grids. The convergence of global relative error with respect to the total number of grid points is also investigated.

2. Petrov-Galerkin NEM Approximation of 2-D Linear Elasticity Problem

Referring to Fig. 1, let us consider a 2-D linear elastic body with a crack which occupies an open bounded domain

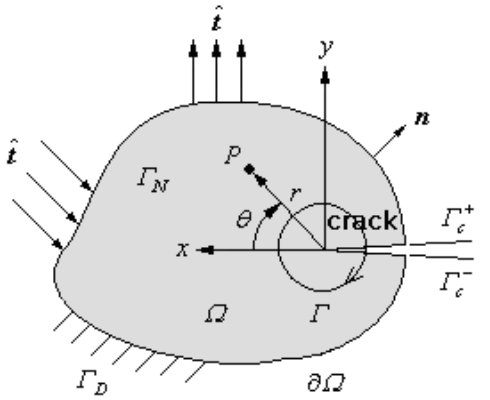

Fig. 1 A 2-D linear elastic body with an edge crack

$\Omega \in \Re^2$ with the boundary $\partial\Omega = \overline{\Gamma_D \cup \Gamma_N \cup \Gamma_c}$, where Γ_D denotes the displacement boundary, Γ_N the traction boundary, and $\Gamma_c = \overline{\Gamma_c^+ \cup \Gamma_c^-}$ the crack surfaces. Assuming the crack surface is traction-free, the displacement field $\boldsymbol{u}(\boldsymbol{x})$ is governed by the static equilibrium

$$\nabla \cdot \boldsymbol{\sigma} = 0 \quad in \quad \Omega \tag{1}$$

with the displacement boundary condition

$$\boldsymbol{u} = \hat{\boldsymbol{u}} \quad on \quad \Gamma_D \tag{2}$$

and the traction boundary condition given by

$$\boldsymbol{\sigma} \cdot \boldsymbol{n} = \begin{cases} \hat{\boldsymbol{t}} & on \quad \Gamma_N \\ 0 & on \quad \Gamma_c^{\pm} \end{cases} \tag{3}$$

In which $\boldsymbol{\sigma}$ indicates the Cauchy stress and $\boldsymbol{n}$ the outward unit vector normal to $\partial\Omega$ and $\hat{\boldsymbol{t}}$ the surface force.

By assuming small displacement and strains, the Cauchy strain $\boldsymbol{\varepsilon}$ is defined by the (3×2) gradient-like operator $\boldsymbol{L}$ such that

$$\varepsilon = \varepsilon(\boldsymbol{u}) = \boldsymbol{L}\boldsymbol{u} \tag{4}$$

Letting $\boldsymbol{D}$ be the (3×3) constitutive matrix, the stresses and strains are constituted by

$$\boldsymbol{\sigma} = \boldsymbol{D} : \boldsymbol{\varepsilon} \tag{5}$$

The boundary value problem (1) is converted to the weak form according to the virtual work principle: Find $\boldsymbol{u}(\boldsymbol{x})$ such that

$$\int_{\Omega} \varepsilon(\boldsymbol{v}) : \sigma(\boldsymbol{u}) d\Omega = \int_{\Gamma_N} \hat{\boldsymbol{t}} \cdot \boldsymbol{v}\, ds \tag{6}$$

for every admissible displacement field $\boldsymbol{v}(\boldsymbol{x})$ in the Cartesian coordinate system $\{x,y\}$. In order for the Petrov-Galerkin natural element approximation using a given non-convex natural element grid $\Im_{NEM}$ composed of N nodes and a number of Delaunay triangles as shown in Fig. 2(a), trial and test displacement fields $\boldsymbol{u}(\boldsymbol{x})$ and $\boldsymbol{v}(\boldsymbol{x})$ are expanded as

$$\boldsymbol{u}_h(\boldsymbol{x}) = \sum_{J=1}^{N} \boldsymbol{u}_J \phi_J(\boldsymbol{x}) = \boldsymbol{\Phi}\bar{\boldsymbol{u}}\,,$$
$$\boldsymbol{v}_h(\boldsymbol{x}) = \sum_{I=1}^{N} \boldsymbol{v}_I \psi_I(\boldsymbol{x}) = \boldsymbol{\Psi}\bar{\boldsymbol{v}} \tag{7}$$

with Laplace interpolation functions $\phi_J(\mathbf{x})$ shown in Fig. 2(b) and three-node triangle-based constant strain (CS)-FE basis functions $\Psi_I(\mathbf{x})$ (Ergun and Ates 2015). The reader may refer to the references (Sukumar *et al.* 1998, Cho and Lee 2006) for more details on the concept of natural element method. Meanwhile, Φ and Ψ denote (2×2N) matrices containing N basis functions ϕ_J and ψ_I, and $\bar{\boldsymbol{u}}$ and $\bar{\boldsymbol{v}}$ are the (2N×1) nodal vectors, respectively.

Substituting Eq. (7) into Eqs. (4)-(5) and (6) leads to

$$\sum_{I}^{N} \boldsymbol{K}^I \bar{\boldsymbol{u}} = \sum_{I}^{N} \boldsymbol{F}^I \tag{8}$$

with the node-wise matrices defined by

$$\boldsymbol{K}^I = \int_{\Omega_v^I} (\boldsymbol{L}\Psi)^T \boldsymbol{D}(\boldsymbol{x})(\boldsymbol{L}\Phi)\, d\Omega \tag{9}$$

$$\boldsymbol{F}^I = \int_{\Gamma_N \cap \Omega_v^I} \Psi^T \hat{\boldsymbol{t}}\, ds \tag{10}$$

in which $\Omega_v^I = supp(\psi_I(\boldsymbol{x}))$ is the support of I-th CS-FE basis function (i.e., a Delaunay triangle), and two matrices Ψ and Φ are defined by

$$\Psi = \left[\begin{pmatrix} \psi_1 & 0 \\ 0 & \psi_1 \end{pmatrix} \cdots \begin{pmatrix} \psi_I & 0 \\ 0 & \psi_I \end{pmatrix} \cdots \begin{pmatrix} \psi_N & 0 \\ 0 & \psi_N \end{pmatrix} \right] \tag{11}$$

$$\Phi = \left[\begin{pmatrix} \phi_1 & 0 \\ 0 & \phi_1 \end{pmatrix} \cdots \begin{pmatrix} \phi_J & 0 \\ 0 & \phi_J \end{pmatrix} \cdots \begin{pmatrix} \phi_N & 0 \\ 0 & \phi_N \end{pmatrix} \right] \tag{12}$$

The numerical integration in the natural element method is carried out Delaunay triangle by Delaunay triangle.

The Petrov-Galerkin natural element (PG-NE) method employs the Delaunay triangle-based CS-FE basis functions to expand the test displacement field. The main reason is to achieve both the numerical integration accuracy and the easy implementation of conventional Gauss quadrature rule (Cho and Lee 2006). The numerical integration in most meshfree methods is usually performed by applying the conventional Gauss quadrature rule to an extra background mesh which is additionally generated. But, differing from other meshfree methods, natural element method does not need additional effort to construct an extra background mesh because Delaunay triangles which are generated *a priori* during the process for defining the Laplace interpolation functions automatically construct a background mesh. Furthermore, the support of CS-FE basis functions is composed of a union of Delaunay triangles, so that the intersection between the CS-FE basis function ψ_I and Laplace basis function ϕ_J is always contained within

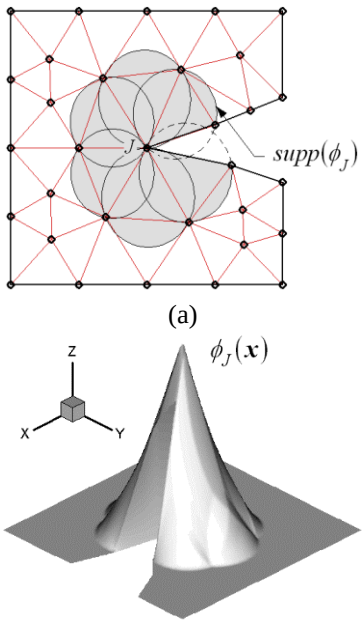

Fig. 2(a) Non-convex NEM grid $\Im_{NEM}$ consisted of Delaunay triangles, (b) Laplace interpolation function $\phi_J(\mathbf{x})$ at the crack tip

Delaunay triangles. Therefore, one can accurately and easily integrate $\boldsymbol{K}^I$ in Eq. (9) by applying the Gauss quadrature rule to each Delaunay triangle, as in the finite element method.

3. Interaction integral in natural element method

Referring to Fig. 1, for two-dimensional planar configuration, the rate of released energy per unit crack extension in the x-direction can be defined by the J-integral formulation given by

$$J = \int_{\Gamma} \left(W\delta_{1j} - \sigma_{ij} \frac{\partial u_i}{\partial x_1} \right) n_j\, ds \tag{13}$$

where $W=\sigma\cdot\varepsilon/2$ is the strain energy density and σ_{ij} are Cauchy stresses evaluated along an arbitrary contour Γ enclosing the crack tip in a counter-clock wise sense. The integral is independent of the choice of contour and the integrand is determined by the natural element analysis. For a mixed-mode crack problem, J is related to the stress intensity factors such that $J = \left(K_I^2 + K_{II}^2\right)/\bar{E}$, according to Irwin's relation (Irwin 1957). In which $\bar{E}$ becomes E for plane stress and $E/(1-\nu^2)$ for plane strain, respectively.

In order to extract K_I and K_{II}, the interaction integral (Shih and Asaro 1988, Daimon and Okada 2014) which considers two equilibrium states of a cracked body is employed. State 1 is the actual equilibrium state of a body subject to the prescribed boundary conditions while state 2 denotes an auxiliary equilibrium state which will be chosen as the asymptotic fields for mode I or II. Then, the J-integral for the sum of the two equilibrium states is

expressed by

$$J^{(1+2)} = \int_{\Gamma}\left[\frac{1}{2}\left(\sigma_{ij}^{(1)}+\sigma_{ij}^{(2)}\right)\left(\varepsilon_{ij}^{(1)}+\varepsilon_{ij}^{(2)}\right)\delta_{1j} - \left(\sigma_{ij}^{(1)}+\sigma_{ij}^{(2)}\right)\frac{\partial\left(u_i^{(1)}+u_i^{(2)}\right)}{\partial x_1}\right]n_j ds$$
$$= J^{(1)} + J^{(2)} + M^{(1,2)} \quad (14)$$

Here, the interaction integral denoted by $M^{(1,2)}$ for the two equilibrium states is defined by

$$M^{(1,2)} = \int_{\Gamma}\left[W^{(1,2)}\delta_{1j} - \sigma_{ij}^{(1)}\frac{\partial u_i^{(2)}}{\partial x_1} - \sigma_{ij}^{(2)}\frac{\partial u_i^{(1)}}{\partial x_1}\right]n_j ds \quad (15)$$

with $W^{(1,2)}$ being the mutual strain energy defined by $W^{(1,2)} = \left[\boldsymbol{\sigma}^{(1)}\cdot\boldsymbol{\varepsilon}^{(2)} + \boldsymbol{\sigma}^{(2)}\cdot\boldsymbol{\varepsilon}^{(1)}\right]/2$. And, it is related to the stress intensity factors K_I and K_{II} in modes I and II as following

$$M^{(1,2)} = \frac{2}{\overline{E}}\left(K_I^{(1)}K_I^{(2)} + K_{II}^{(1)}K_{II}^{(2)}\right) \quad (16)$$

Referring to Anderson (1991), the closed form near-tip displacement fields for modes I and II in two-dimensional linear fracture mechanics are available. And, the mode I stress intensity factor $K_I^{(1)}$ for state 1 can be determined by making state 2 as the pure mode I asymptotic field with $K_I^{(2)} = 1$

$$M^{(1,\text{ModeI})} = \frac{2}{\overline{E}}K_I^{(1)} \quad (17)$$

In a similar manner, the stress intensity factor K_{II} of mode II can be also determined (i.e., $M^{(1,ModeII)} = 2K_{II}^{(1)}/\overline{E}$).

The line integral (15) is not best for numerical calculation because the integration of displacement gradients, strains and stresses of states 1 and 2 along path Γ is rather painstaking. Thus, it is desired to be transformed into an area integral form, for which Eq. (15) is firstly rewritten as

$$M^{(1,2)} = \int_{C}\left[\sigma_{ij}^{(1)}\frac{\partial u_i^{(2)}}{\partial x_1} + \sigma_{ij}^{(2)}\frac{\partial u_i^{(1)}}{\partial x_1} - W^{(1,2)}\delta_{1j}\right]qm_j ds \quad (18)$$

by substituting the path Γ with $C = \Gamma + \Gamma_c^- + \Gamma_c^+ + \Gamma_o$ as shown in Fig. 3 and by multiplying a sufficiently smooth weighting function $q(x)$. The weighting function has unity on Γ, zero on Γ_o, and arbitrary value between 0 and 1 within the interior domain A. By taking the divergence theorem to Eq. (18) and letting the inner path Γ be shrunk to the crack tip, the interaction integral ends up with

$$M^{(1,2)} = \int_{A}\left[\sigma_{ij}^{(1)}\frac{\partial u_i^{(2)}}{\partial x_1} + \sigma_{ij}^{(2)}\frac{\partial u_i^{(1)}}{\partial x_1} - W^{(1,2)}\delta_{1j}\right]\frac{\partial q}{\partial x_j}dA \quad (19)$$

Meanwhile, the integral domain A and the weighting function $q(x)$ for the interaction integral (19) are constructed by specifying a domain defining radius r_{int} as shown in Fig. 4. The value of unity is assigned to all the nodes within the circle, while the value of zero is specified to the remaining nodes within a NEM grid. Then, a union of interior

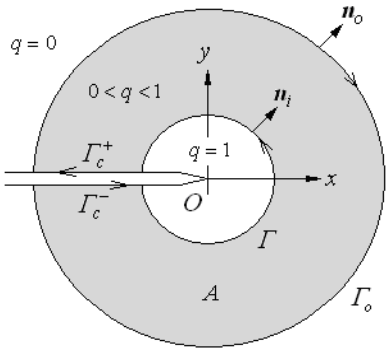

Fig. 3 An extended closed path and the integral domain A

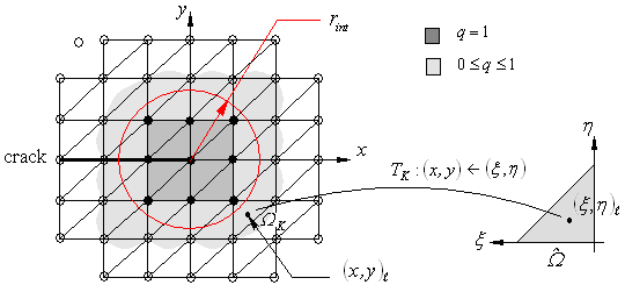

Fig. 4 The integral domain A and the weighting function $q(x)$ by a domain defining circle

darkened eight Delaunay triangles generates a rectangular and its boundary serves as an interior path Γ shown in the previous Fig. 3. In addition, one can define another union of grayed Delaunay triangles in which only one or two nodes have the value of unity, and its boundary becomes the outer path Γ_o. Hence, the union of grayed Delaunay triangles automatically becomes an integral domain A, where the weighting function $q(x)$ has the value between zero and unity. The interaction integral $M^{(1,2)}$ is numerically calculated by applying the Gauss quadrature rule to the Delaunay triangles within the integral domain A.

4. Near-tip grid refinement in NEM

In this section, the proposed near-tip grid refinement for the natural element method is described in detail. A NEM grid is composed of finite number of nodes and Delaunay triangles, as represented in Fig. 5(a). As addressed in earlier, the near-tip refinement is performed in two steps and the first step is schematically represented in Fig. 5, where *nd_crk* indicates the crack tip node. The darkened eight triangles are to be divided into sixteen sub-triangles, as represented in Fig. 5(b). In addition, a grid point (i.e., node) is to be created at the intersecting point of four sub-triangles, resulting in a creation of four nodes and eight sub-triangles in the first refinement step. The radial distances r_1 of four grid points from the crack tip node are the same.

Referring to Fig. 6, the global node numbers are assigned to the four created nodes in a manner of NODE+1, NODE+2, NODE+3 and NODE+4 with NODE being the total number of nodes in a NEM grid before refinement. As well, the global element numbers are assigned to the eight

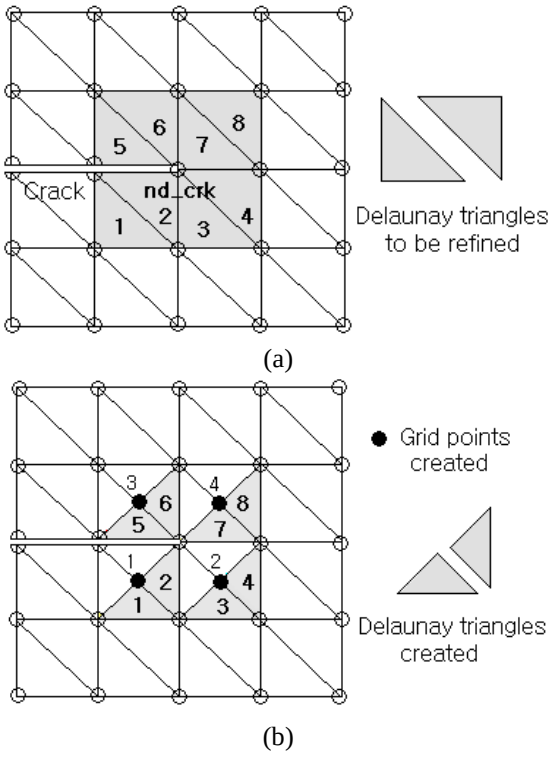

Fig. 5 First refinement: (a) selection of near-tip Delaunay triangles, (b) creation of 4 grid points and 8 Delaunay triangles

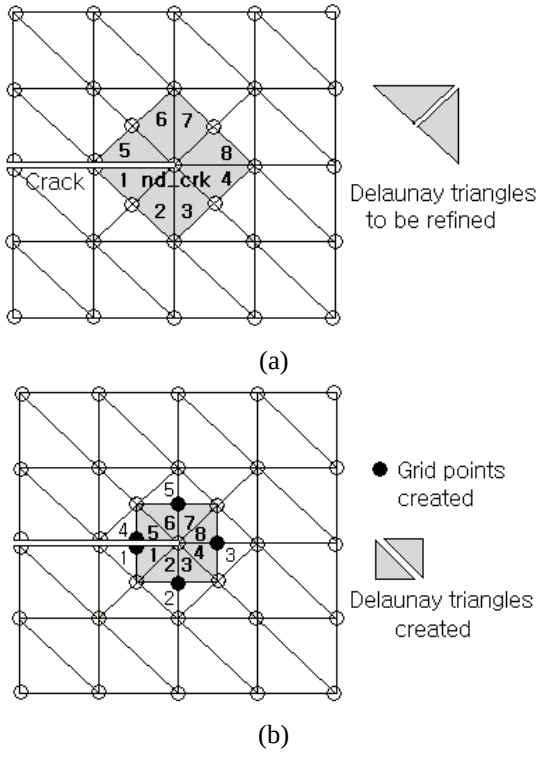

Fig. 7 Second refinement: (a) selection of near-tip Delaunay triangles, (b) creation of 5 grid points and 8 Delaunay triangles

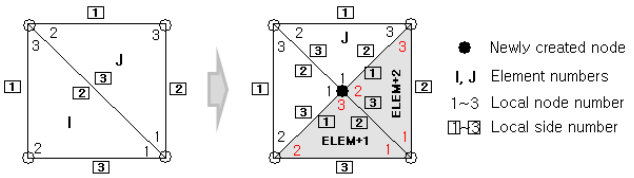

Fig. 6 Specification of local node numbers and neighbor elements for newly created triangular elements

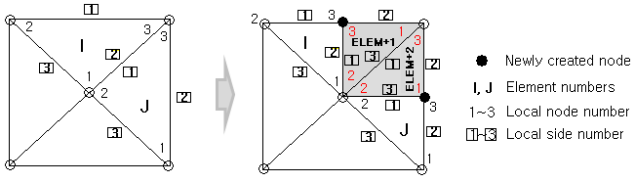

Fig. 8 Specification of local node numbers and neighbor elements for newly created triangular elements

created sub-triangles in the similar manner of ELEM+1, . . . , ELEM+8 with ELEM being the total number of triangles in a NEM grid before refinement. Meanwhile, for the sixteen sub-triangles, the local node numbers are updated or newly assigned starting from 1 to 3 clockwise. In addition, the neighbor element information is assigned to three local sides of each sub-triangle. Where, 1, 2 and 3 mean the local node numbers where the global node numbers are assigned, while 1, 2 and 3 in rectangles indicate the three sides of triangle where the neighbor element numbers are assigned. The neighbor element number becomes 0 when no neighbor element exists on the local side.

The second near-tip grid refinement is represented in Fig. 7, where eight triangles are chosen for further division. Eight triangles are divided into sixteen sub-triangles, as in the first refinement, but five grid points are created because two nodes are needed for the two crack faces. The radial distances r_2 of five nodes from the crack tip node are the same. The suitable values of the radial distances r_1 and r_2 will be determined through the preliminary experiment in the next section 5. The global node numbers for five created nodes and the global element numbers for eight created triangles are assigned in the same manner for the previous first refinement. As a result, the total numbers of nodes and triangular elements which were created through the first and second grid refinement are nine and sixteen respectively. Fig. 8 represents the update or newly assignment of local node numbers and neighbor element numbers for the newly created eight sub-triangles.

5. Numerical experiments

The near-tip grid refinement algorithm was coded in Fortran and combined into our in-house PG-NEM program in which an interaction integral module (Cho and Lee 2014) and a patch recovery module (Cho 2016) were built in. As a numerical example for benchmark test, a rectangular plate shown in Fig. 9 with symmetric edge cracks is taken, which is in the plane strain state and subject to uniform vertical distributed load σ_∞. The material properties are as follows: E=200 *Gpa* and v=0.3. This problem was firstly tested by Tracey (1971) and later revisited by Barsoum (1976) for the numerical study using the singular quadratic iso-parametric

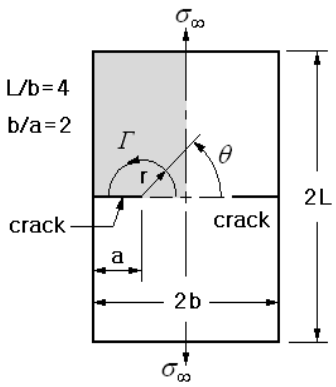

Fig. 9 A plane strain rectangular plate with symmetric edge cracks (unit: *m*)

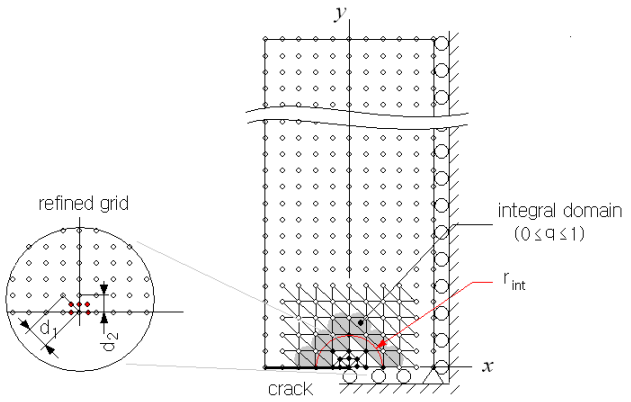

(a)

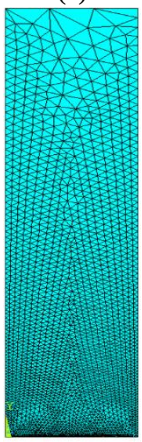

(b)

Fig. 10 NEM grids: (a) uniform grid with near-tip refinement, (b) fine gradient grid generated by utilizing ANSYS (*N*=2,516)

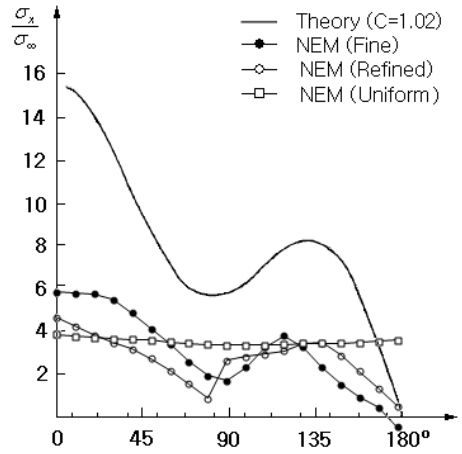

(a)

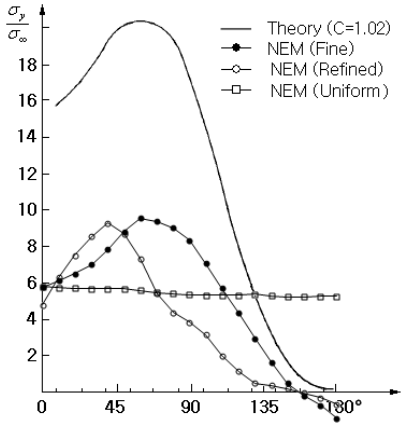

(b)

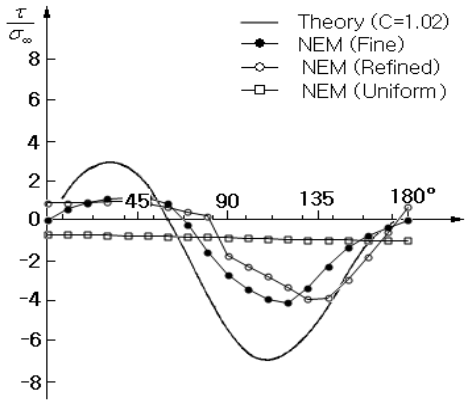

(c)

Fig. 11 Comparison of stress distributions along the circular path Γ (r/a=0.0139): (a) σ_{xx}, (b) σ_{yy}, and (c) τ_{xy}

elements. A darkened quarter is taken for the crack analysis from the symmetry of problem.

Three different NEM grids were used for the crack analysis, 11×41 uniform grid, 11×41 uniform grid plus near-tip refinement shown Fig. 10(a), and a gradient fine grid shown in Fig. 10(b). The gradient fine grid was generated with the help of ANSYS such that the grid density increases towards the crack tip. Both the uniform and fine grids were used for the comparison purpose. In Fig. 10(a), four nodes and eight sub-triangles were created near the crack tip according to the first and second grid refinement. And, the radial distances r_1 and r_2 were set by 1/10 of the distances d_1 and d_2, from the parametric preliminary experiment. It has been observed that the numerical accuracy decreases when the radial distance becomes smaller than 1/10 of d_1 and d_2. Meanwhile, r_{int} indicates the domain defining radius, which was introduced in Fig. 4, for the interaction integral. It was set by two times of the square of the area of a rectangular element composed of two Delaunay triangles (Moës *et al.* 1999).

Table 1 The computed absolute and relative errors to the NEM grid density

NEM grid	Absolute error $\|\hat{\boldsymbol{u}}-\boldsymbol{u}_h\|_{E(\Omega)}$		Relative error ξ_G (%)	
	Uniform	Locally refined	Uniform	Locally refined
3×9	1.182E-05	1.642E-05	20.565	18.141
7×25	1.129E-05	1.049E-05	13.908	11.592
11×41	9.929E-06	8.322E-06	10.968	9.193
17×65	7.964E-06	6.693E-06	8.798	7.394
21×81	7.174E-06	6.042E-06	7.926	6.675

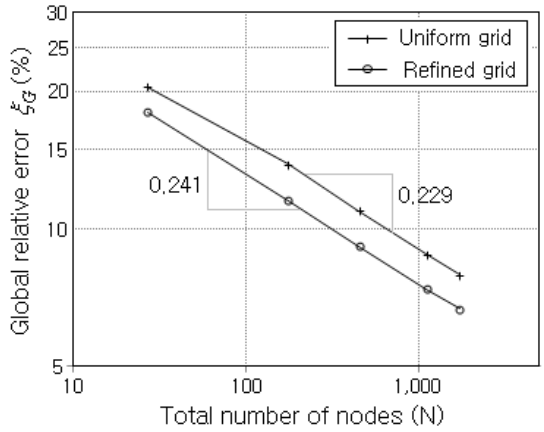

Fig. 12 Comparison of convergence rates between uniform and locally refined NEM grids

The crack analyses were performed for all three NEM grids, and next the bare stress fields which were obtained by direct differentiating the approximated displacement fields were smoothened and enriched through the stress recovery. The numerical integration for both the crack analyses and the stress recovery was carried out with 13 Gaussian points. Figs. 11(a)-(c) comparatively represent the distributions of dimensionless relative stresses along the circular path Γ shown in Fig. 9, where the radius r was set by 0.0139a. The stress intensity factor for this problem is expressed by (with the correction factor C of 1.02 (ASTM 1965),

$$K_I = \sigma_\infty \sqrt{\pi a}\left(\frac{2b}{\pi a} tan\frac{\pi a}{2b}\right)\cdot C \tag{20}$$

so that the near-tip stress field is analytically possible. First of all, it is found that the uniform NEM grid show almost uniform distributions which are totally different from the exact ones. But, the gradient fine grid shows the distributions similar to the exact ones even though the levels are lower than the exact ones. This trend can be also found from the distributions which were obtained using the refined grid. Thus, the effectiveness of the proposed near-tip refinement has been clearly justified that the refined grid can represent the near-tip stress distributions similar to those obtained using the gradient fine grid, even with grid points less than 20% of the total nodes of gradient fine grid.

Next, the global error analyses were carried out for uniform and refined grids. Letting $\hat{\boldsymbol{u}}$ be the displacement field obtained using the gradient fine grid, the absolute global error $\|\hat{\boldsymbol{u}}-\boldsymbol{u}_h\|_{E(\Omega)}$ in the energy norm is defined by

$$\|\hat{\boldsymbol{u}}-\boldsymbol{u}_h\|^2_{E(\Omega)} = \frac{1}{2}\int_\Omega (\hat{\boldsymbol{\varepsilon}}-\boldsymbol{\varepsilon}_h)\cdot(\hat{\boldsymbol{\sigma}}-\boldsymbol{\sigma}_h)dA \approx |U(\hat{\boldsymbol{u}})-U(\boldsymbol{u}_h)| \tag{21}$$

with $U(\cdot)$ being the total strain energy $\boldsymbol{u}_h$ being the displacement fields obtained using refined and uniform grids. Meanwhile, the global relative error ξ_G is defined by

$$\xi_G = \frac{\|\hat{\boldsymbol{u}}-\boldsymbol{u}_h\|_{E(\Omega)}}{U(\hat{\boldsymbol{u}})^{1/2}}\times 100\% \approx \left(\frac{|U(\hat{\boldsymbol{u}})-U(\boldsymbol{u}_h)|}{U(\hat{\boldsymbol{u}})}\right)^{1/2}\times 100\% \tag{22}$$

Note that the solution obtained using the gradient fine grid is assumed to be an exact solution because the exact displacement field is not accessible.

The computed absolute and relative errors for uniform and refined grids are recorded in Table 1 with respect to the density of NEM grid. For all the NEM grids, it is observed that the errors of the near-tip refined grid are smaller than those of uniform grid. Meanwhile, both errors of uniform and refined grids show the monotonic decrease in proportional to the grid density. Fig. 12 represents the log-log scale of the global relative error ξ_G with respect to the total node number N. It is found that the convergence rates (the slope of two plots) are almost similar for both NEM grids, even though the refined grid shows smaller errors for the whole range of total node number.

Table 2 The computed mode-I SIFs $K_I/\sigma_\infty\sqrt{\pi a}$ with respect to the crack length

Method		Crack length a						
		4	6	8	10	12	14	16
Theory (C=1.02)		1.0549	1.1028	1.1795	1.2987	1.4896	1.8206	2.4981
NEM	Uniform	0.9806	1.0007	1.0430	1.2437	1.4789	1.9294	2.5746
	Refined	1.0933	1.1001	1.1199	1.2854	1.4224	1.7992	2.4582

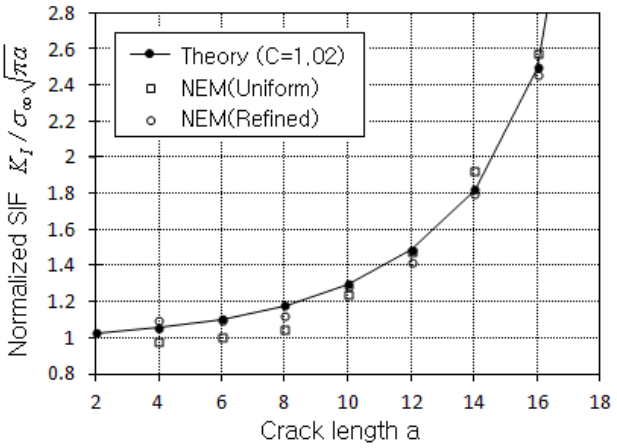

Fig. 13 Variation of the normalized mode-I stress intensity factor $K_I/\sigma_\infty\sqrt{\pi a}$ to the crack length a

Next, the stress intensity factors (SIF) K_I were calculated using uniform and refined grids and compared with the exact ones given in Eq. (20). The normalized mode-I SIFs $K_I / \sigma_\infty \sqrt{\pi a}$ with respect to the crack length a are compared in Table 2. It is found that the near-tip refined grid leads to the SIFs close to the exact ones than uniform grid, such that the maximum relative errors are 5.05% for the refined grid and 11.57% for uniform grid. The variation of normalized SIFs is represented in Fig. 13, where the better prediction accuracy of the refined grid is clearly observed, except for the crack length a of 12. Thus, it has been justified that the near-tip refined grid leads to smaller error in the prediction of neat-tip stresses and SIFs, for all the grid densities and the crack lengths.

4. Conclusions

In this paper, a near-tip grid refinement method has been introduced for the reliable and effective crack analysis by the natural element method (NEM). The Delaunay triangles sharing the crack tip node were divided into two sub-triangles, and grid points (i.e., nodes) were newly created at the centers of squares built with four sub-triangles. This grid refinement was accomplished in two subsequent steps, with a uniform NEM grid. The radial distances r_1 and r_2 of newly created nodes from the crack tip node were set by 1/10 of the diagonal lengths d_1 and d_1 of triangles. The validity and usefulness of the proposed refinement method have been justified through the crack analyses of a plane rectangle with symmetric edge cracks. The crack analyses were carried out using three types of NEM grids, uniform, gradient fine and near-tip refined grids, for the sake of comparison purpose.

From the comparison of stress distributions around the crack tip, the uniform grid showed the totally different distribution, but the near-tip refined grid lead to the distribution quite similar to one of the gradient fine grid, even with grid points less than 20% of the total nodes of gradient fine grid. This enrichment of near-tip stress field by the proposed refinement was also confirmed from the error analysis. The refined grid shows smaller errors for the whole range of total node number, even though the convergence rate is almost similar to one of uniform grid. Furthermore, it has been justified that the near-tip refined grid leads to the SIFs more close to the exact ones than uniform grid, such that the maximum relative errors are 5.05% at the refined grid and 11.57% at uniform grid.

However, the proposed method is limited to the regular NEM grid so that the extension to the irregular NEM grid deserves the research topic for future work.

Acknowledgements

This research was supported by Basic Science Research Program through the National Research Foundation of Korea (NRF) funded by the Ministry of Education (Grant No. NRF-2017R1D1A1B03028879).

References

Anderson, T.L. (1991), *Fracture Mechanics: Fundamentals and Applications*, 1st Edition, CRC Press.

Areias, P., Rabczuk, T. and De Sa, J.C. (2016), "A novel two-stage discrete crack method based on the screened Poisson equation and local mesh refinement", *Comput. Mech.*, **58**(6), 1003-1018. https://doi.org/10.1007/s00466-016-1328-5.

ASTM (1965), "Fracture toughness testing and its applications", *ASTM Spec. Tech. Pub.*, **381**, 43-51.

Barsoum, R.S. (1976), "On the use of isoparametric finite elements in linear fracture mechanics", *Int. J. Numer. Meth. Eng.*, **10**(1), 25-37. https://doi.org/10.1002/nme.1620100103.

Belytschko, T., Lu, Y.Y., Gu, L. and Tabbara, M. (1995), "Element-free Galerkin methods for static and dynamic fracture", *Int. J. Sol. Struct.*, **32**(17-18), 2547-2570. https://doi.org/10.1016/0020-7683(94)00282-2.

Braun, J. and Sambridge, M. (1995), "A numerical method for solving partial differential equations on highly irregular evolving grids", *Nat.*, **376**(6542), 655-660. https://doi.org/10.1038/376655a0.

Cao, Z. and Liu, Y. (2012), "A new numerical modelling for evaluating the stress intensity factors in 3-D fracture analysis", *Struct. Eng. Mech.*, **43**(3), 321-336. https://doi.org/10.12989/sem.2012.43.3.321.

Chinesta, F., Cescotto, S., Cueto, E. and Lorong, P. (2011), *Natural Element Method for the Simulation of Structures and Processes*, John Wiley & Sons, New Jersey, U.S.A.

Ching, H.K. and Batra, R.C. (2011), "Determination of crack tip fields in linear elastostatics by the meshless local Petrov-Galerkin (MLPG) method", *Comput. Model. Eng. Sci.*, **2**(2), 273-289.

Cho, J.R. and Lee, H.W. (2006), "A Petrov-Galerkin natural element method securing the numerical integration accuracy", *J. Mech. Sci. Technol.*, **20**(1), 94-109. https://doi.org/10.1007/BF02916204.

Cho, J.R. and Lee, H.W. (2014), "Calculation of stress intensity factors in 2-D linear fracture mechanics by Petrov-Galerkin natural element method", *Int. J. Numer. Meth. Eng.*, **98**(11), 819-839. https://doi.org/10.1002/nme.4666.

Cho, J.R. (2016), "Stress recovery techniques for natural element method in 2-D solid mechanics", *J. Mech. Sci. Technol.*, **30**(11), 5083-5091. https://doi.org/10.1007/s12206-016-1026-4.

Daimon, R. and Okada, H. (2014), "Mixed-mode stress intensity factor evaluation by interaction integral method for quadratic tetrahedral finite element with correction terms", *Eng. Fract. Mech.*, **115**, 22-42. https://doi.org/10.1016/j.engfracmech.2013.11.009.

Erdogan, F. and Wu, B.H. (1997), "The surface crack problem for a plate with functionally graded properties", *ASME J. Appl. Mech.*, **64**(3), 449-456. https://10.1115/1.2788914.

Ergun, M. and Ates, S. (2015), "The stress analysis of a shear wall with matrix displacement method", *Struct. Eng. Mech.*, **53**(2), 205-226. https://doi.org/10.12989/sem.2015.53.2.205.

Fleming, M., Chu, Y.A., Moran, B. and Belytschko, T. (1997), "Enriched element-free Galerkin methods for crack tip fields", *Int. J. Numer. Meth. Eng.*, **40**(8), 1483-1504. https://doi.org/10.1002/(SICI)1097-0207(19970430)40:8<1483::AID-NME123>3.0.CO;2-6.

Goli, E., Bayesteh, H. and Mohammadi, S. (2014), "Mixed mode fracture analysis of adiabatic cracks in homogeneous and non-homogeneous materials in the framework of partition of unity and the path-independent interaction integral", *Eng. Fract. Mech.*, **131**, 100-127. https://doi.org/10.1016/j.engfracmech.2014.07.013.

Hou, C., Wang, Z., Liang, W., Yu, H. and Wang, Z. (2017), "Investigation of the effects of confining pressure on SIFs and

T-stress for CCBD specimens using the XFEM and the interaction integral method", *Eng. Fract. Mech.*, **178**, 279-300. https://doi.org/10.1016/j.engfracmech.2017.03.049.

Irwin, G.R. (1957), "Analysis of stresses and strains near the end of a crack traveling a plate", *J. Appl. Mech.*, **24**, 361-364.

Kim, J.H. and Paulino, G.H. (2002), "Finite element evaluation of mixed mode stress intensity factors in functionally graded materials", *Int. J. Numer. Meth. Eng.*, **53**(8), 1903-1935. https://doi.org/10.1002/nme.364.

Lo, S.H. and Lee, C.K. (1992), "Solving crack problems by an adaptive refinement procedure", *Eng. Fract. Mech.*, **43**(2), 147-163. https://doi.org/10.1016/0013-7944(92)90118-X.

Moës, N., Dolbow, J. and Belytschko, T. (1999), "A finite element method for crack growth without remeshing", *Int. J. Numer. Meth. Eng.*, **46**(1), 131-150. https://doi.org/10.1002/(SICI)1097-0207(19990910)46:1<131::AID-NME726>3.0.CO;2-J.

Pant, M., Singh, I.V. and Mishra, B.K. (2011), "A novel enrichment criterion for modeling kinked cracks using element free Galerkin method", *Int. J. Mech. Sci.*, **68**, 140-149. https://doi.org/10.1016/j.ijmecsci.2013.01.008.

Rabczuk, T. and Belytschko, T. (2004), "Cracking particles: A simplified meshfree method for arbitrary evolving cracks", *Int. J. Numer. Meth. Eng.*, **61**(13), 2316-2343. https://doi.org/10.1002/nme.1151.

Rao, B.N. and Rahman, S. (2000), "An efficient meshless method for fracture analysis of cracks", *Comput. Mech.*, **26**(4), 398-408. https://doi.org/10.1007/s004660000189.

Shi, J., Ma, W. and Li, N. (2013), "Extended meshless method based on partition of unity for solving multiple crack problems", *Meccan.*, **43**(9), 2263-2270. https://doi.org/10.1007/s11012-013-9743-6.

Shih, C.F. and Asaro, R.J. (1998), "Elasto-plastic analysis of cracks on biomaterial interfaces: Part I-small scale yielding", *J. Appl. Mech.*, **55**, 299-316.

Solanki, S., Daniewicz, S.R. and Newman Jr, J.C. (2003), "Finite element modeling of plasticity-induced crack closure with emphasis on geometry and mesh refinement effects", *Eng. Fract. Mech.*, **70**(12), 1475-1489. https://doi.org/10.1016/S0013-7944(02)00168-6.

Sukumar, N., Moran, A. and Belytschko, T. (1998), "The natural element method in solid mechanics", *Int. J. Numer. Meth. Eng.*, **43**(5), 839-887. https://doi.org/10.1002/(SICI)1097-0207(19981115)43:5<839::AID-NME423>3.0.CO;2-R.

Sukumar, N. and Moran, A. (1999), "C^1 natural neighbor interpolant for partial differential equations", *Numer. Meth. Part. Diff. Eqs.*, **15**(4), 417-447. https://doi.org/10.1002/(SICI)1098-2426(199907)15:4<417::AID-NUM2>3.0.CO;2-S.

Szabó, B. and Babuška, I. (1991), *Finite Element Analysis*, John Wiley & Sons, New York, U.S.A.

Tong, P., Pian, T.H.H. and Lasry, S.J. (1973), "A hybrid element approach to crack problems in plane elasticity", *Int. J. Numer. Meth. Eng.*, **7**(3), 297-308. https://doi.org/10.1002/nme.1620070307.

Tracey, D.M. (1971), "Finite elements for determination of crack tip elastic stress intensity factors", *Eng. Fract. Mech.*, **3**(3), 255-265. https://doi.org/10.1016/0013-7944(71)90036-1.

Xiao, Q.Z., Karihaloo, B.L. and Liu, X.Y. (2004), "Direct determination of SIF and higher order terms of mixed mode cracks by a hybrid crack element", *Int. J. Fract.*, **125**(3-4), 207-225. https://doi.org/10.1023/B:FRAC.0000022229.54422.13.